

The Eurasia Proceedings of Science, Technology, Engineering & Mathematics (EPSTEM), 2022

Volume 17, Pages 6-18

ICRETS 2022: International Conference on Research in Engineering, Technology and Science

Synthesis of Iron-containing Nanoparticles from Iron-Steel Industrial Waste for Adsorption of Malachite Green

Deniz UZUNOGLU

Mersin University

Ayla OZER

Mersin University

Abstract: For the synthesis of iron-containing nanoparticles (FeNPs), the iron ions were recovered from iron-steel industrial waste by leaching method followed by the chemical precipitation of ferric hydroxide with NH_3 . The ferric hydroxide was reduced pyrometallurgical to iron-containing nanoparticles by the reducing agent of CO generated from charcoal. FeNPs were characterized by XRD and SEM analysis. XRD results showed that FeNPs had predominantly face-centered cubic Fe_3O_4 structure, besides, the peaks of Fe_2O_3 and Fe^0 structures were also observed. The particle size of FeNPs was calculated as 57.75 nm using Williamson–Hall equation. According to SEM images, FeNPs had homogeneous and spherical-like structures; also, the structures partially decomposed and the particle size increased due to the agglomeration of the particles after adsorption. FeNPs were used as an adsorbent for the removal of Malachite Green (MG). The experimental design and the optimization of experimental conditions were investigated by using response surface methodology (RSM) according to central composite design (CCD). The optimum experimental conditions were determined as 180 min contact time, 75 °C temperature, and 300 mg/L initial MG concentration. The agreement between the adsorbed MG concentrations at the equilibrium (q_e) calculated from the model (148.43 mg/g) and determined experimentally (146.63 mg/g) under the optimum conditions showed that the selected model was suitable for MG adsorption by FeNPs. Langmuir isotherm model had higher R^2 and lower ARE values than Freundlich isotherm model, showing that the equilibrium data of MG adsorption with FeNPs was the best agreement to Langmuir isotherm model with the maximum monolayer coverage capacity of 175.44 mg dye/g FeNPs. The thermodynamic studies suggested that the adsorption process was endothermic, spontaneous at the optimum conditions, and the positive ΔS value indicated the increased disorder at the solid-solution interface during the adsorption.

Keywords: Iron-containing nanoparticles, Pyrometallurgical nanoparticle synthesis, Response surface methodology, Adsorption, Malachite Green

Introduction

Textile industries consume large quantities of water and so large quantities of wastewater containing synthetic dyes causing significant environmental pollution due to their toxic, carcinogenic, teratogenic or mutagenic nature were discharged into receiving water environment (Deb et al., 2021). These dyes have a non-biodegradable and stable against oxidizing agents structure, which makes them difficult to remove from the aqueous solutions. Color is the first detectable contaminant in this type of wastewaters and should be removed before it is discharged into receiving water environment. There are several physical, chemical, biological, and advanced separation methods for color removal, which is listed in Table 1 (Gadekar & Ahammed, 2019). Among the methods listed in Table 1, adsorption has a long-standing background and still continues to attract great attention due to some advantages such as low cost, a wide variety of adsorbents, high removal efficiency, regeneration possibility, and lower energy requirement (Harja et al., 2022).

- This is an Open Access article distributed under the terms of the Creative Commons Attribution-Noncommercial 4.0 Unported License, permitting all non-commercial use, distribution, and reproduction in any medium, provided the original work is properly cited.

- Selection and peer-review under responsibility of the Organizing Committee of the Conference

© 2022 Published by ISRES Publishing: www.isres.org

Table 1. Color removal methods

Physical methods	Chemical methods	Biological methods	Advanced methods
Sedimentation Float (Flotation) Membrane processes	Oxidation	Aerobic/anaerobic treatment	Improved ultrafiltration
	Chemical Precipitation		Electrodialysis
	Electrochemical degradation	Activated sludge process	Integrated chemical- biological degradation
	Chemical reduction/oxidation		Reverse osmosis Ion exchange Adsorption

The types and properties of adsorbents affect adsorption processes. There are various adsorbent types used in the adsorption of dyes from wastewaters and they are listed in Table 2 (Harja et al., 2022). Among them, nanomaterials have higher adsorption capacities than the others due to their higher surface/volume ratio. Nanomaterials can be synthesized by physical, chemical, and biological methods or hybrid methods that are combinations of several of them (Patra & Baek, 2014). The synthesis costs of nanomaterials with high adsorption capacity are relatively high and this cost can be reduced by using agricultural or industrial waste. The iron-steel industry produces tons of waste materials containing iron oxides, heavy metals, and other different contaminants. Disposing of them in landfills causes environmental pollution because they release toxic substances to soil and groundwater (Kargin et al., 2022). Iron-steel slag has the most significant industrial waste volumes and more than 400 million tons of iron and steel slag were produced worldwide in 2017. If such a large volume of waste materials is effectively recycled, not only the environmental pollution and disposal costs would reduce, but also new cheap technologies would assert for developing advanced materials such as micro/nano materials (Schoeman et al., 2021). With this viewpoint, in this study, iron-containing nanoparticles, a synthetic adsorbent, were synthesized via chemical precipitation followed by pyrometallurgical reduction with the intent of converting an industrial waste to a value-added advanced product. In addition to these studies, the experimental design, the optimization of experimental conditions, and the two-way interaction between the independent variables were investigated by using response surface methodology (RSM) according to central composite design (CCD) for the adsorption of MG by FeNPs. Response surface methodology (RSM) is a widely-used statistical technique applied in order to optimize independent variables to achieve maximum or minimum response through a series of experiments. There are some limitations of the conventional optimization technique of the one-factor variable approach such as the requirement of a large number of experimental data and inadequate explanation of the interactive relation between multiple process parameters. These limitations of the conventional technique can be overcome by optimizing all the independent variables collectively by central composite experimental design via RSM, which reduces the runs of experiments resulting in cost and timesaving. So, RSM has been frequently used in the optimization of the adsorption process in recent years (Deb et al., 2021; Nguyen et al., 2022).

Table 2. Adsorbent types

Natural adsorbents	Synthetic adsorbents	Agricultural waste	Industrial waste
Algae Clays Zeolites Silicon ores Iron oxides	Activated carbon	Sawdust	Waste paper
	Fullerenes	Wood splinter	Cotton linter waste
	Hydrochar	Tree bark	Waste cigarette filters
	Chitin/chitosan	Cone	Fly ash
	Hydroxyapatite	Fruit and vegetable peels	Iron-steel industrial waste
	Polymers	Nut shells	Red mud
	Micro/nano materials	Wheat straw	Metal hydroxide waste
	Micro/nano composites	Rice husk	Aluminum sulphate waste
		Corn cob	Treatment sludge
		Sugarcane pulp	waste tire
	Animal pulp	Blast furnace slag	

Method

Synthesis and Characterization of Iron-containing Nanoparticles

For the synthesis of iron-containing nanoparticles (FeNPs); the components in the iron-steel industrial waste were firstly leach out by treatment with HCl, then a precipitation was formed by NH₃ solution, and finally FeNPs were synthesized via the pyrometallurgical reduction using charcoal as the reductant agent. Accordingly;

the iron-steel industrial waste and concentrated HCl solution (35 wt%) were mixed in an Erlenmeyer-flask at a ratio of solid:liquid=1:6 and this mixture was magnetically stirred for 1 h at 80 °C for leaching out the components in the waste into HCl. After cooling of the resulting mixture, the acid insoluble residue was separated by centrifuge at 3460 RCF for 5 min and the obtained leach solution was analyzed by Inductively Coupled Plasma-Mass Spectrometer (ICP-MS, Agilent, Japan). Then, the desired amount of concentrated NH₃ solution (25 wt%) was added to the leach solution until the precipitate formation was over. The formed precipitate as a result of the reaction between NH₃ and the leach solution was separated by centrifuge at 3460 RCF for 5 min, washed with 1.0% HCl followed by distilled water to remove the excess NH₃ and soluble impurities and finally dried in the stove at 105°C for 12 h. After that, FeNPs were synthesized via pyrometallurgical reduction method using charcoal and the obtained precipitate. Accordingly, certain amounts of the precipitate and charcoal were taken into porcelain crucibles separately, and they were heated in the muffle furnace at 1200 °C for 4 h. FeNPs formed as a result of the reaction between the precipitate and CO generated from the charcoal. Finally, the obtained FeNPs were washed with distilled water and dried in the stove at 105°C for 12 h (Giri et al., 2011). The synthesized FeNPs were characterized with X-ray diffractometer (XRD) and scanning electron microscopy (SEM). The XRD pattern was collected on a Rigaku (Japan) diffractometer with CuK α radiations in diverse angle range (2 θ) of 10–90°, operating at the tube voltage of 40 kV and a tube current of 30 mA. The morphological examination was performed on Zeiss (Germany) field emission scanning electron microscopy.

Experimental Design and Optimization using Response Surface Methodology

The experimental design and the optimization of experimental conditions of the adsorption of MG by FeNPs were investigated by using response surface methodology (RSM) according to central composite design (CCD). The independent variables were chosen as contact time, temperature, and initial dye concentration; and the adsorbed dye amount per gram of adsorbent at the predetermined contact time (Y:mg dye/g adsorbent) was set down as dependent response variable. The ranges and the levels of the independent variables for the adsorption of MG by FeNPs are presented in Table 3.

Table 3. The ranges and the levels of the independent variables for the adsorption of MG by FeNPs

Symbol	Independent variable	Coded ranges and levels		
		Low (-1)	Center (0)	High (+1)
A	Contact time (min)	10	95	180
B	Temperature (°C)	25	50	75
C	Initial dye concentration (mg/L)	100	200	300

Table 4. The experimental design and the responses for the adsorption of MG by FeNPs

Run order	Independent variables and responses				Run order	Independent variables and responses			
	A	B	C	Y		A	B	C	Y
1	95	25	200	39.21	21	10	25	300	0.43
2	95	50	200	79.48	22	10	25	300	0.45
3	180	50	200	85.84	23	10	75	100	4.82
4	95	50	300	93.37	24	180	25	100	25.96
5	95	75	200	91.27	25	10	75	100	4.75
6	95	50	100	47.37	26	95	50	200	79.33
7	95	25	200	39.50	27	180	25	100	25.81
8	95	75	200	89.19	28	95	50	200	78.53
9	180	50	200	85.82	29	95	50	200	78.69
10	95	50	200	78.66	30	180	25	300	95.40
11	95	50	200	78.63	31	10	25	100	0.33
12	95	50	200	78.84	32	180	25	300	92.65
13	95	50	300	94.00	33	95	50	200	78.56
14	10	50	200	2.77	34	10	25	100	0.32
15	95	50	100	47.43	35	10	75	300	40.51
16	10	50	200	2.83	36	95	50	200	79.15
17	95	50	200	79.74	37	180	75	100	51.42
18	180	75	300	146.94	38	10	75	300	40.52
19	95	50	200	78.80	39	180	75	100	51.28
20	180	75	300	146.86	40	95	50	200	79.15

The experimental design as well as the responses for the effect of three independent variables in 40 runs of experiments were given in Table 4. The obtained responses were treated to develop an empirical model which correlated the response to the independent variables using a second-degree polynomial equation as given by the following equation (Dargahi et al., 2021):

$$Y = \beta_0 + \sum_{i=1}^k \beta_i x_i + \sum_{i=1}^k \beta_{ii} x_i^2 + \sum_{i=1}^{k-1} \sum_{j=i+1}^k \beta_{ij} x_i x_j + \varepsilon \quad \text{Eq. (1)}$$

where Y is the predicted response, β_0 is the constant coefficient, β_i is the linear coefficient, β_{ij} is the interaction coefficient, β_{ii} is the quadratic coefficient, x_i and x_j are the coded values of the adsorption of MG by FeNPs. The interaction between the independent variables and the responses were tested by using ANOVA and the effect of the variables was also evaluated with response surface graphs.

Adsorption of Malachite Green by FeNPs

The experiments of the adsorption of MG by FeNPs were carried out according to the central composite design matrix given in Table 4. The adsorption experiments were performed out in Erlenmeyer flasks (250 mL) containing 100 mL of MG dye solutions. 1.0 g/L of the adsorbent (FeNPs) was blended with MG dye solution at natural pH and known initial MG concentration (100–300 mg/L). Then, the flasks were shaken in the agitation vessel at desired temperatures and constant shaking rate. The samples were taken at the predetermined contact time and then were separated from the adsorbent by centrifugation at 3460 RCF for 5 min. The unadsorbed MG dye concentration in supernatant was analyzed at 618 nm wavelength with UV–vis spectrophotometer. Experiments were repeated for different contact time, temperature, and initial dye concentration values (Karacabey et al., 2019). The adsorbed dye amount per gram of adsorbent at the predetermined contact time, q_t (mg/g), was calculated as follows:

$$q_t = (C_0 - C_t) / X_0 \quad \text{Eq. (2)}$$

where C_0 is the initial dye concentration (mg/L), C_t is the dye concentration at the predetermined contact time (mg/L), and X_0 is the adsorbent concentration (g/L).

Results and Discussion

Synthesis Steps of FeNPs

The illustration of the synthesis steps of FeNPs was presented in Figure 1. In order to explain the formation of FeNPs, the prepared leach solution was analyzed by ICP-MS and the results were given in Table 5. The results of ICP-MS showed that the obtained leach solution was in the form of FeCl_3 in view of the mole ratio between Fe and Cl ions. In the formation step of FeCl_3 , the ferric iron (Fe^{3+}) was firstly recovered from the iron-steel industrial waste, and then the experiment was continued for the reaction between Fe^{3+} and HCl to take place resulting in FeCl_3 . After that, NH_3 solution was added to FeCl_3 solution until the precipitate formation was over; in this step, the reaction took place between NH_3 and FeCl_3 resulting in ferric hydroxide. In the last synthesis step, the pyrometallurgical reduction was carried out in the muffle furnace. Accordingly, CO formed as a result of the combustion of coal, and the resulting CO reduced the ferric hydroxide to form FeNPs.

Table 5. ICP-MS results of the leach solution

Element	mg/L	Number of Moles
Cl	170.2	
Mg	104.3	
Fe	89.37	
Cr	74.83	Base: 1 L solution
Ca	68.79	Number of Moles (n): (Mass)/(Molar Mass)
Na	42.87	$n_{\text{Cl}}: (170.2 \text{ mg}) / (35.5 \text{ mg/mmol}) = 4.79 \text{ mmole}$
Al	10.77	$n_{\text{Fe}}: (89.37 \text{ mg}) / (55.84 \text{ mg/mmol}) = 1.60 \text{ mmole}$
Si	1.132	Empirical formula: $\text{Fe}_{1.6}\text{Cl}_{4.79} \sim \text{FeCl}_3$
Zn	1.093	
Ti	0.773	
Cu	0.489	

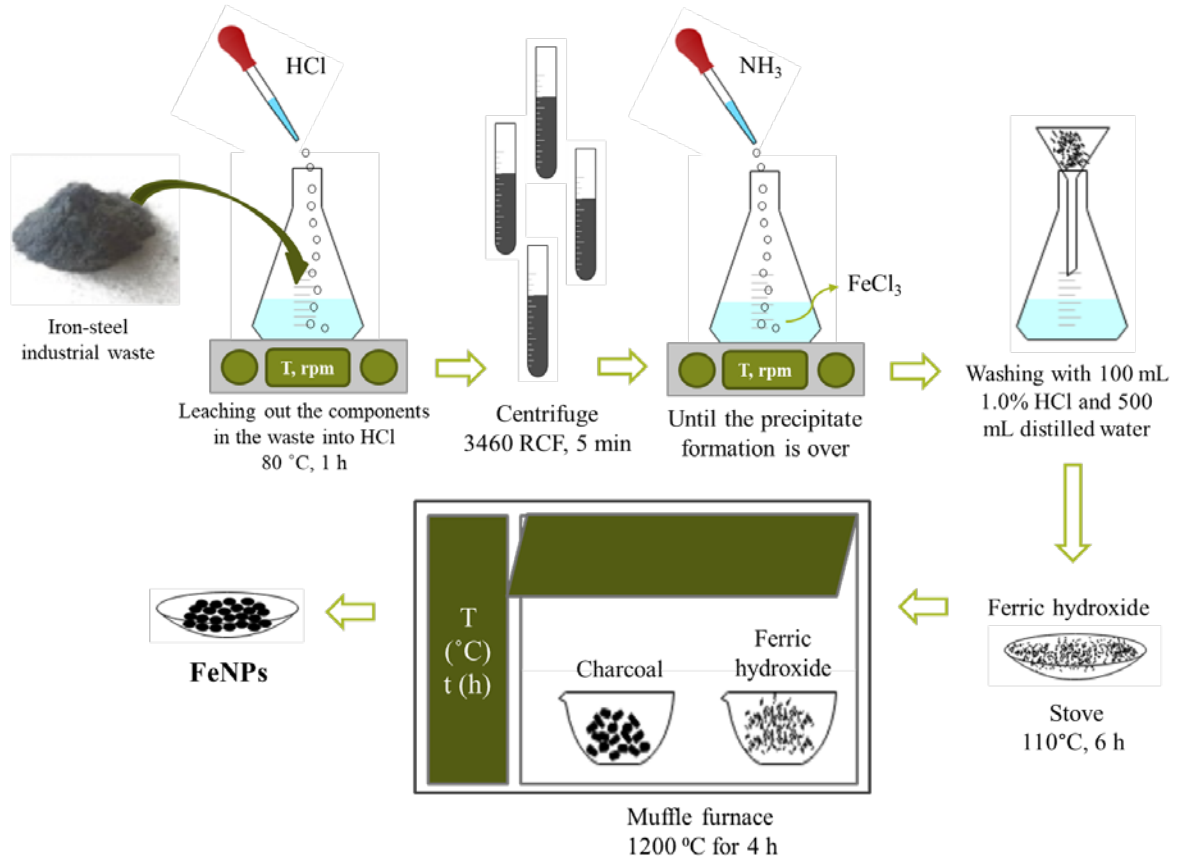


Figure 1. The synthesis steps of FeNPs

Characterization of FeNPs

XRD analysis was carried out to determine the crystal structure and phase state of FeNPs. The characteristic peaks in XRD pattern of FeNPs (Figure 2) belong to the phases of Fe₃O₄, Fe₂O₃, and Fe⁰ (Gandha et al., 2016; Khuyen et al., 2018) were given in Table 6.

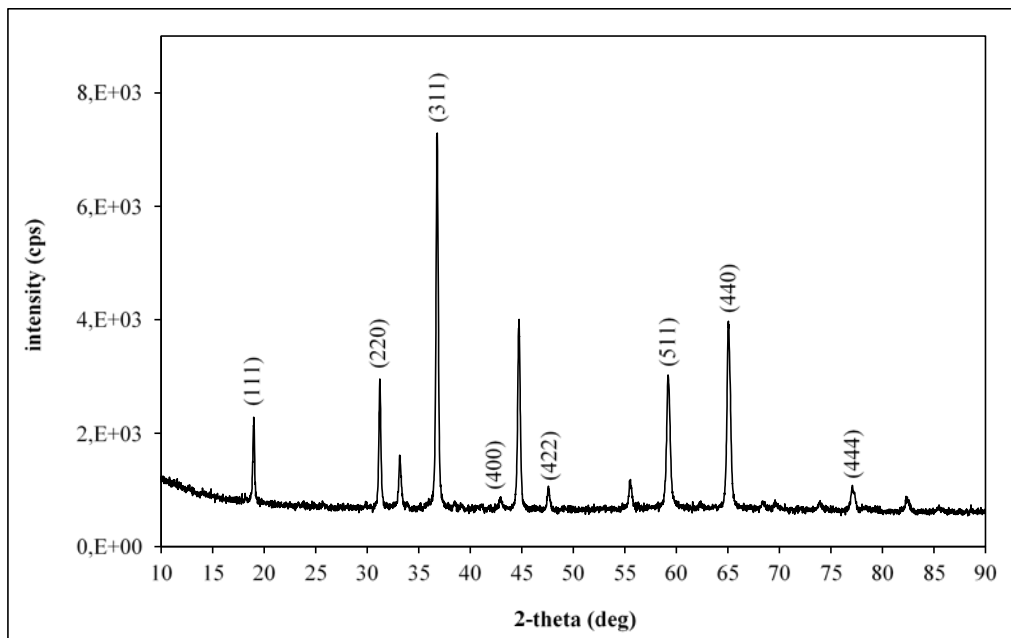


Figure 2. XRD pattern of FeNPs

Table 6. The characteristic peaks of the different phases of FeNPs

Phase	Plane	2-theta (deg)
Fe ₃ O ₄	(111)	18.99°
	(220)	31.22°
	(311)	36.77°
	(400)	42.98°
	(422)	55.49°
	(511)	59.19°
	(440)	65.05°
	(444)	77.08°
Fe ₂ O ₃	(104)	33.14°
	(110)	36.77°
	(024)	47.57°
Fe ⁰	(116)	55.49°
	(110)	44.69°
	(211)	82.36°

The particle size of FeNPs was calculated using the obtained characteristic XRD peaks according to Williamson–Hall equation given below (Irfan et al., 2018; Kahouli et al., 2015):

$$\beta \cdot \cos\theta = (K\lambda/D) + 4 \varepsilon \cdot \sin\theta \quad \text{Eq. (3)}$$

where β is the expanded diffraction peak measured at FWHM (in radians), θ is the diffraction angle of Bragg, K is the shape factor ($K=0.9$), λ is the X-ray wavelength ($\text{CuK}\alpha=0.154 \text{ nm}$), D is the crystallite size (nm), and ε is the average strain.

By plotting $4 \cdot \sin\theta$ vs $\beta \cdot \cos\theta$, the crystalline size and the average strain can be found by the Y-intercept extrapolation and the slope of the line given in Figure 3. Accordingly, the crystalline size of FeNPs and the average strain were calculated to be 57.75 nm and 0.0065.

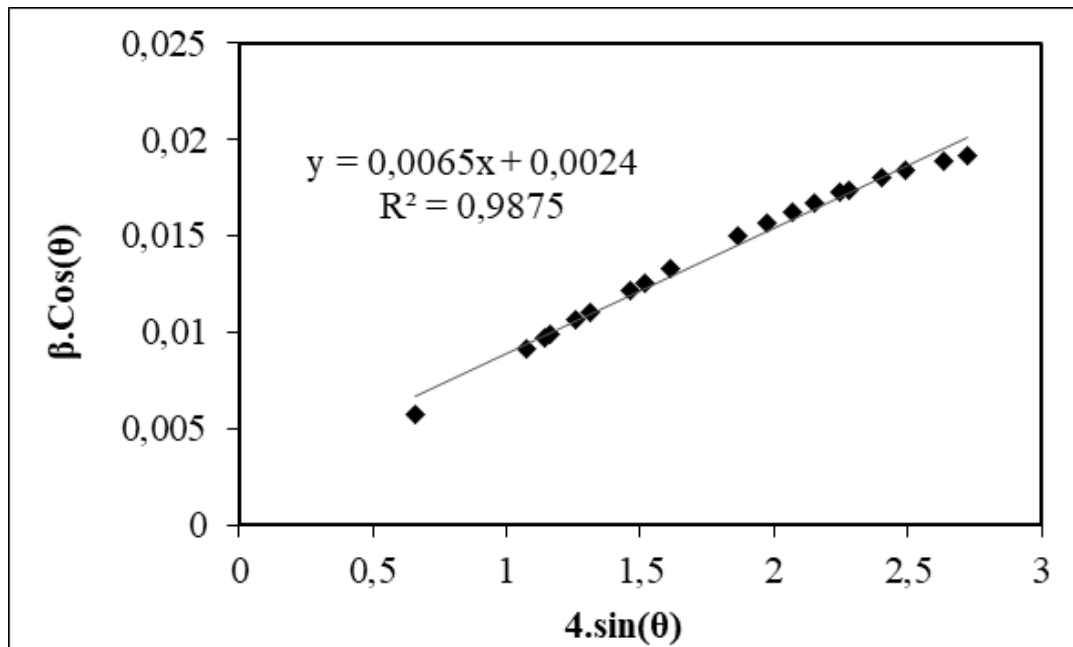


Figure 3. Williamson–Hall plot

The morphology of FeNPs was investigated with SEM, and SEM images before and after adsorption were presented in Figure 4. (a) and (b). According to Figure 4. (a), FeNPs had a homogeneous appearance and their structures were similar to spherical. It was observed that large structures were formed due to the agglomeration. In addition, the average particle size of FeNPs was calculated as 54.83 nm with Image-J program, that was consistent with the value calculated using Williamson–Hall equation (57.75 nm). According to SEM image of FeNPs after adsorption Figure 4. (b), it was observed that the structure of FeNPs partially deteriorated after adsorption and the particle size increased due to the agglomeration.

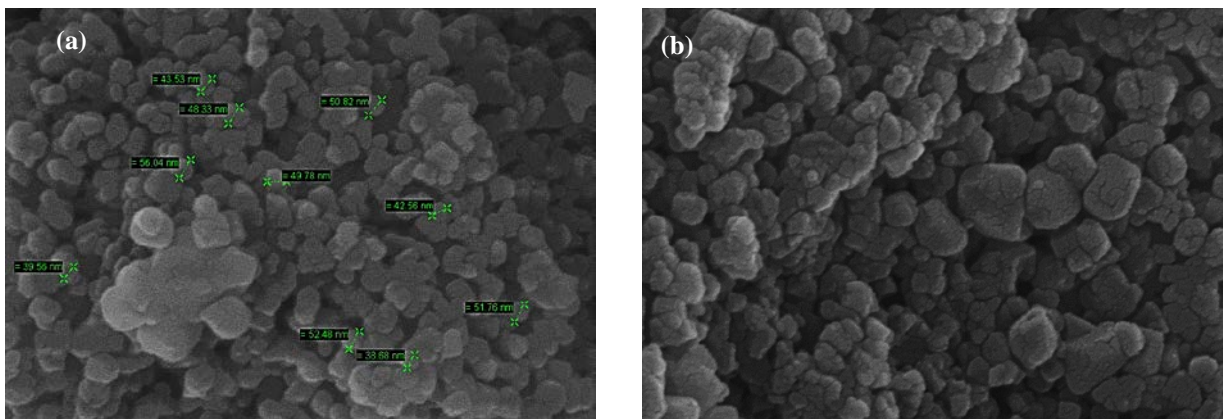


Figure 4. SEM images of FeNPs (a) before adsorption and (b) after adsorption

Adsorption Studies

Optimization of the Experimental Conditions of the Adsorption of MG by FeNPs

The effects of experimental conditions such as contact time, temperature, and initial dye concentration on the adsorption of MG by FeNPs were investigated by using RSM according to CCD. The second-degree polynomial equation expressing the relation between the independent variables and the response for this study was given below.

$$Y = -33.8 + 0.6574 A + 0.949 B - 0.0520 C - 0.003763 A^2 - 0.01073 B^2 - 0.000096 C^2 + 0.001989 AB + 0.001880 AC + 0.003151 BC \quad \text{Eq. (4)}$$

The F-test was used for statistical significance analysis of variance (ANOVA) of the quadratic model equation and the ANOVA results were given in Table 7. Accordingly, the F values of linear, square, and two-way interaction models were found to be 573.84, 111.27, and 71.02, respectively, also all P values of the models were lower than 0.0001.

Table 7. ANOVA results of the quadratic model

Source	Degree of freedom	Sum of squares	Mean square	F-value	P-value	Remarks
Model	11	57733.5	5248.5	208.45	<0.0001	Significant
Linear	3	43346.2	14448.7	573.84	<0.0001	Significant
A	1	25223.3	25223.3	1001.76	<0.0001	Significant
B	1	6037.9	6037.9	239.80	<0.0001	Significant
C	1	12084.9	12084.9	479.96	<0.0001	Significant
Square	3	8404.9	2801.6	111.27	<0.0001	Significant
AA	1	3968.7	3968.7	157.62	<0.0001	Significant
BB	1	241.5	241.5	9.59	0.004	-
CC	1	4.9	4.9	0.20	0.662	-
Two-way interaction	3	5364.7	1788.2	71.02	<0.0001	Significant
AB	1	285.8	285.8	11.35	0.002	-
AC	1	4086.0	4086.0	162.28	<0.0001	Significant
BC	1	992.9	992.9	39.43	<0.0001	Significant
Error	28	705.0	25.2	*	*	*
Lack of fit	5	697.2	139.4	409.16	<0.0001	Significant
Pure error	23	7.8	0.3	*	*	*
Total	39	58438.5	*	*	*	*

$R^2=0.9879$; $R_{adj}^2=0.9832$; $R_{pred}^2=0.9760$

It revealed that linear, quadratic, and two-way interaction models were statistically significant. The variance analysis of the experimental design showed that the terms of A, B and C in linear model; the term of AA in the

quadratic model; the terms of AC and BC in the two-way interaction model were significant. The regression coefficient (R^2) was found to be 0.9879, showing that 98.79% of the variability in response was explained by the model. Figure 5 represented the relationship between predicted Y values (theoretically calculated transformed values) and actual Y values (experimentally transformed values). The data points were found to be close to linear ($R^2=0.9879$), indicating the good correlation between the predicted and the experimental responses. Also, the difference between $R_{pred}^2 = 0.9760$ and $R_{adj}^2 = 0.9832$ was acceptable. As a result, the quadratic model provided an adequate estimate of the adsorption of MG by FeNPs.

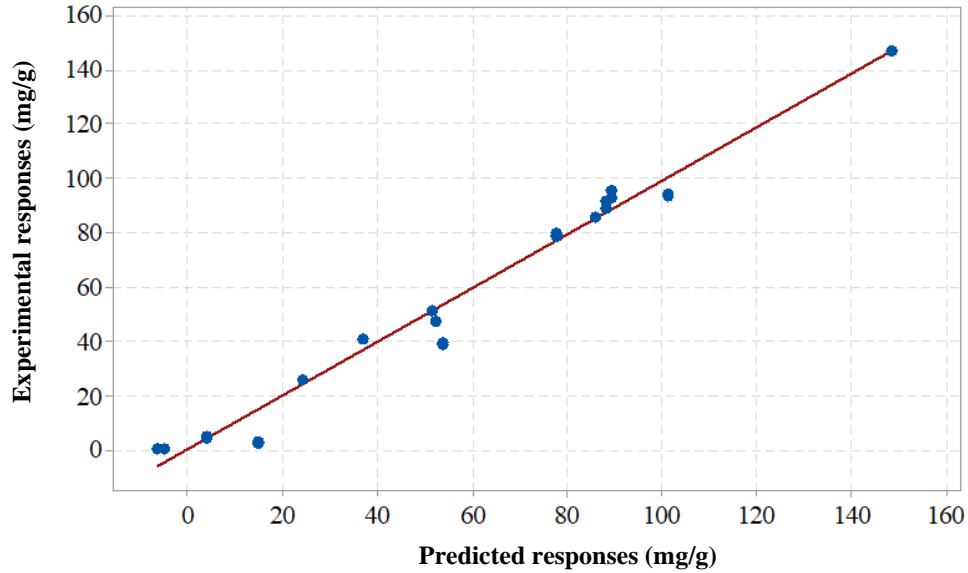


Figure 5. The plot of experimental responses vs predicted responses

The normal probability plot is a graphical technique used to identify important distinctions from normality. In this graph, it is desired that the points are distributed on a straight line (Dargahi et al., 2021). The normal probability graph obtained in this study was presented in Figure 6. It was seen in Figure 6 that the data were normally distributed in this study.

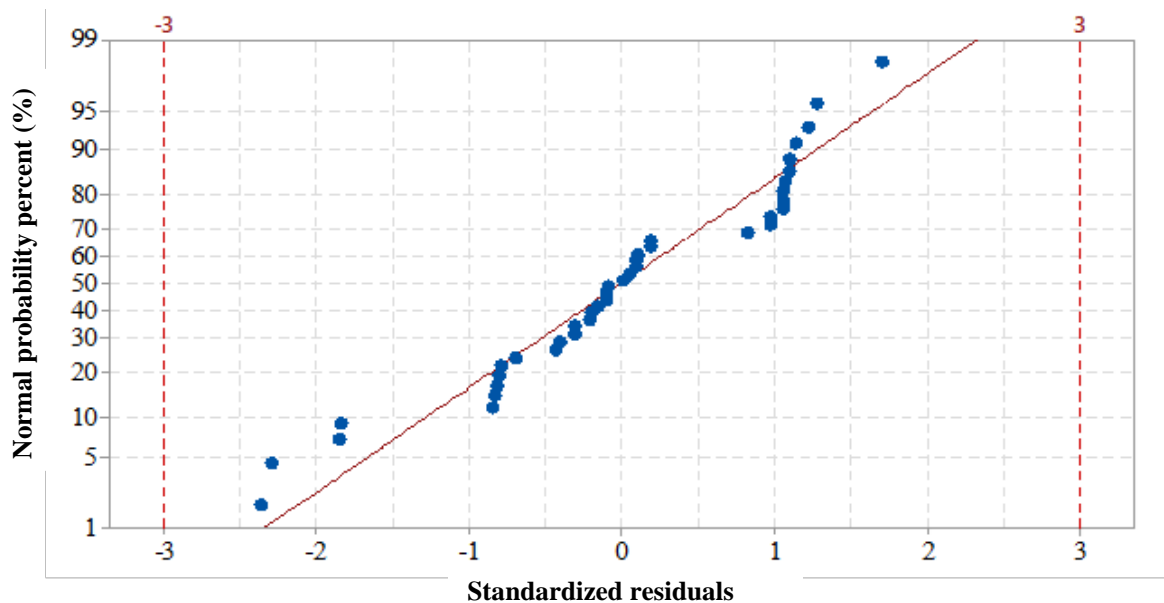


Figure 6. Normal probability plot

The optimum experimental conditions were determined to be 180 min contact time (A), 75°C temperature (B), and 300 mg/L initial MG concentration (C). Under these conditions, the maximum adsorbed MG amount per gram of adsorbent (Y:mg MG/g adsorbent) was determined as 148.43 mg/g from the quadratic model. In order

to prove the accuracy of the model, an experiment was conducted under the optimum experimental conditions and Y value was found to be 146.63 mg/g experimentally. The agreement between the Y values calculated from the model and determined experimentally showed that the selected model was suitable for the adsorption of MG by FeNPs.

In order to investigate the two-way interactions between the independent variables, 3D response surface graphs (Figure 7. (a-c)) were drawn based on the second-degree polynomial equation. In Figure 7. (a), the variation of Y with temperature and initial MG concentration was shown when the other variables were kept constant at the center points. Accordingly, Y values increased with increasing temperature and initial dye concentration. For this reason, the optimum temperature and initial dye concentration were determined as 75°C and 300 mg/L, respectively. As seen in Figure 7. (b), Y values increased with increasing contact time; so, the optimum contact time was determined as 180 min. It was observed in Figure 7. (c) that Y values increased as the contact time and temperature increased.

The increase in Y values as the temperature increases can be attributed to the endothermic nature of the process. On the other hand, as the initial dye concentration increases, more dye molecules are adsorbed on the adsorbent surface and the adsorbed dye amounts increases due to the increase in the driving force (ΔC) in the adsorbate solution. With the increase in the contact time, the active sites of the adsorbent are filled with more dye cations and thus the adsorbed dye amounts increases.

It could be seen in 3D response surface graphs that the two-way interactions in Figure 7. (a) and Figure 7. (b) were more effective on the response than that of Figure 7. (c), as well as the F values of the two-way interactions in Table 7. The F values of the contact time-initial dye concentration (AC) and temperature-initial dye concentration (BC) were greater than that of the contact time-temperature (AB). In addition, while the two-way interactions of the contact time-initial dye concentration (AC) and temperature-initial dye concentration (BC) were significant, the contact time-temperature (AB) two-way interaction was not significant.

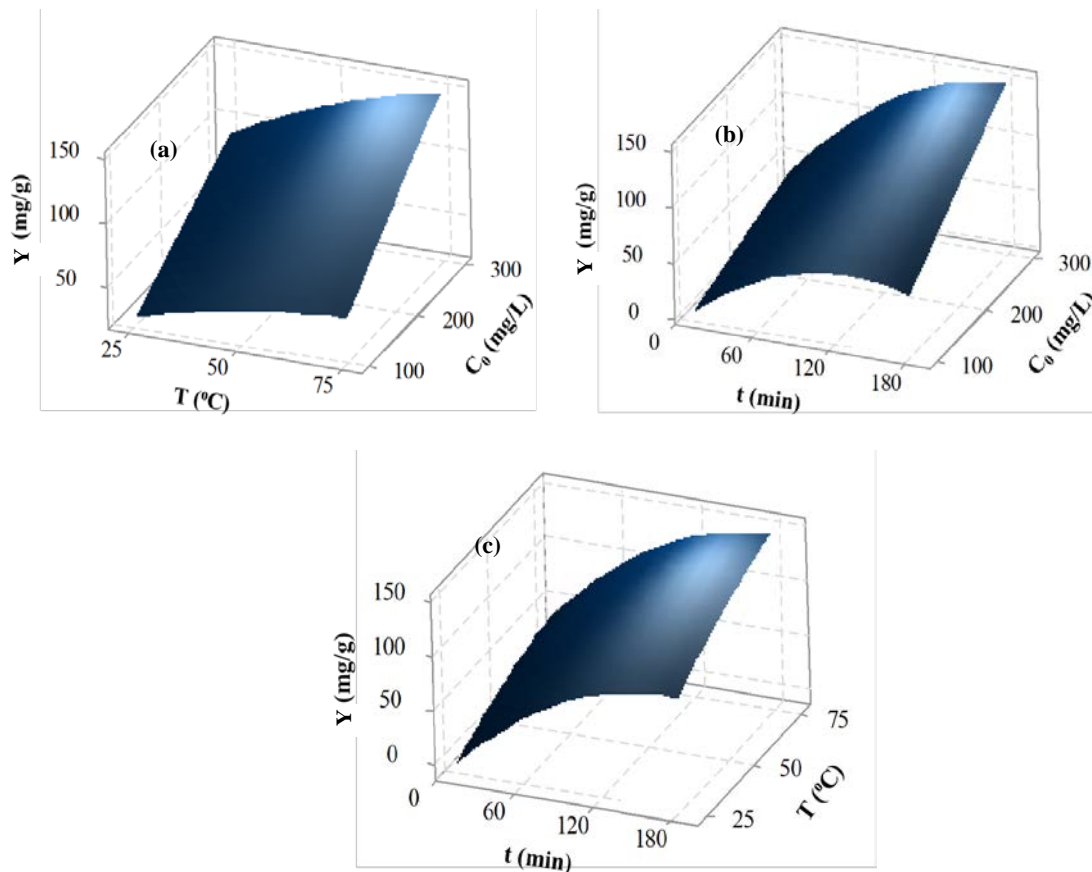


Figure 7. 3D response surface graphs (a) T; Temperature (°C)- C₀; Initial dye concentration (mg/L), (b) t; Contact time (min)- C₀; Initial dye concentration (mg/L), (c) t; Contact time (min)- T; Temperature (°C)

Equilibrium Modelling

Information about the surface properties of the adsorbent, the design of the adsorption process, and the adsorption behavior can be obtained by applying the adsorption isotherms to the equilibrium data. The linear equations of Langmuir and Freundlich isotherm models, which are the most used isotherm models, were given below:

$$[1/q_e] = [1/(Q^0 \cdot b \cdot C_e)] + [1/Q^0] \quad \text{Eq. (5)}$$

$$[\ln q_e] = [\ln K_f] + [(1/n) \cdot (\ln C_e)] \quad \text{Eq. (6)}$$

where q_e (mg/g) and C_e (mg/L) are the adsorbed dye amount per gram of adsorbent and unadsorbed dye concentration in solution at equilibrium, respectively; Q^0 is the maximum monolayer coverage capacity (mg/g) and b is a constant related to the affinity of the binding sites (L/mg); K_f and $1/n$ are the Freundlich constants indicating adsorption capacity and intensity, respectively.

The values of Q^0 and b were calculated from intercept and slope of the linear plot of $1/q_e$ vs. $1/C_e$ (Eq. 5), and the values of K_f and $1/n$ were determined from intercept and slope of the linear plot of $\ln q_e$ vs. $\ln C_e$ (Eq. 6). In this study, the equilibrium data were evaluated with Langmuir and Freundlich isotherm models for different temperatures. The obtained isotherm constants as well as regression coefficients and ARE values were presented in Table 8. Accordingly, the higher R^2 values and the lower ARE values indicated that the equilibrium data could be represented with Langmuir isotherm model than Freundlich isotherm model. It indicated the monolayer adsorption of MG on the homogeneous surface of FeNPs with identical binding sites. In addition, the increase in Q^0 values with the increase in temperature confirmed that the adsorption process was endothermic. The maximum monolayer adsorption capacity (Q^0) of FeNPs was found to be 175.44 mg/g at the optimum temperature of 75°C and compared with the other adsorbents in the literature (Table 9). It could be concluded that FeNPs could be evaluated as an efficient adsorbent for the adsorption of MG due to its relatively high adsorption capacity (Q^0) compared to the other adsorbents in the literature.

Table 8. Isotherm model constants with the values of R^2 and ARE

T (°C)	Langmuir Isotherm Model				Freundlich Isotherm Model			
	Q^0 (mg/g)	b (L/mg)	R^2	ARE	K_f (mg/g)/(L/mg) ^{1/n}	1/n	R^2	ARE
25	89.29	0.006401	0.9997	1.1639	1.39	0.6908	0.9916	4.08
50	92.59	0.864000	0.9995	1.5559	39.65	0.2239	0.8614	15.27
75	175.44	0.438462	0.9996	1.8395	48.70	0.4782	0.9133	16.36

Table 9. The maximum monolayer adsorption capacities (Q^0) of different adsorbents for MG adsorption

Adsorbent	Q^0 (mg/g)	Reference
Corn straw-derived biochar supported nZVI magnetic composite	515.77	(Eltaweil et al., 2020)
Magnetic activated carbon (Fe ₃ O ₄ -AC)	311.40	(Altintig et al., 2018)
FeNPs	175.44	This work
Gold nanoparticles loaded on activated carbon	172.20	(Roosta et al., 2014)
Zinc sulfide:copper nanoparticle loaded on activated carbon	168.07	(Dastkhooon et al., 2015)
Halloysite nanotubes	99.6	(Kiani et al., 2011)
β-cyclodextrin polymer coated Fe ₃ O ₄ magnetic nanoparticles	88.49	(Liang et al., 2018)
Nanoscale zero-valent iron supported by carbonized pomegranate peel	32.47	(Gunduz & Bayrak, 2018)
Bimetallic Fe–Zn nanoparticles	21.74	(Gautam et al., 2015)

Thermodynamic Evaluation

In order to define the thermodynamic behavior of the adsorption of MG by FeNPs, the thermodynamic parameters of Gibb's free energy change (ΔG), enthalpy change (ΔH), and entropy change (ΔS) were calculated using the following equations:

$$\Delta G = -RT \cdot \ln K_c \quad \text{Eq. (7)}$$

$$K_c = C_{ad,e} / C_e \quad \text{Eq. (8)}$$

$$\ln K_c = (\Delta S/R) - (\Delta H/RT) \quad \text{Eq. (9)}$$

where K_c is the equilibrium constant at temperature T , $C_{ad,e}$ is the adsorbed dye concentration at equilibrium (mg/L), C_e is the unadsorbed dye concentration at equilibrium (mg/L), ΔG (J/mole) is the Gibb's free energy change, ΔH (J/mole) is the enthalpy change of the adsorption process, ΔS (J/(mole.K)) is the entropy change of the adsorption process.

The values of ΔH and ΔS can be calculated from the slope and intercept of the linear plot of $\ln K_c$ vs $1/T$, respectively. The calculated thermodynamic parameters were given in Table 10. Accordingly, the adsorption of MG by FeNPs was spontaneous ($\Delta G < 0$) at optimum temperature, increasing in the randomness of adsorbed species ($\Delta S > 0$), and endothermic ($\Delta H > 0$) as predicted in the sections of adsorption studies and equilibrium modeling (Shalaby et al., 2021).

Table 10. The calculated thermodynamic parameters

T (K)	K_c	ΔG (J/mole)	ΔH (J/mole)	ΔS (J/mole.K)
298	0.1193	5267.71		
323	0.8840	331.02	75104.52	233.45
348	9.4639	-6502.57		

Conclusion

This work revealed an applicable method for the evaluation of iron-steel industrial waste in the pyrometallurgical synthesis of a value-added product, iron-containing nanoparticles (FeNPs), for an environmental application of MG adsorption. The crystal and morphological structure of FeNPs synthesized via this route was proved by XRD and SEM analysis. The particle sizes of FeNPs were calculated with Williamson–Hall equation and Image-J program as 57.75 nm and 54.83 nm, respectively. The usability of the synthesized FeNPs in the adsorption of MG was investigated. The experimental design, the effect of independent variables on the response, and the optimization of experimental conditions were investigated with RSM according to CCD by significantly reducing the number of experiments. The optimum experimental conditions were found to be 180 min contact time, 75 °C temperature, and 300 mg/L initial MG concentration. The all independent variables were found to have significant effects on the adsorption of MG by FeNPs at the individual level. The results of ANOVA indicated that the two-way interaction between the contact time and initial dye concentration had the highest effect on the response due to the highest F-value. RSM based optimization revealed that the maximum adsorbed dye amount per gram of adsorbent was determined as 148.43 mg/g at the optimum conditions which was close to the value found experimentally as 146.63 mg/g. It was found that the equilibrium adsorption data were better fitted to the Langmuir isotherm model than the Freundlich isotherm model. The monolayer adsorption capacity obtained at optimum condition ($Q^0=175.44$ mg/g) was competitive with the values reported for the adsorption of MG. Thermodynamic data showed that the adsorption process was endothermic and spontaneous, and the randomness of adsorbed species increased during the adsorption of MG by FeNPs. These results showed that the low-cost FeNPs synthesized from iron-steel industrial waste can be efficiently applied for the adsorption of industrial wastewater containing of MG.

Scientific Ethics Declaration

The authors declare that the scientific ethical and legal responsibility of this article published in EPSTEM journal belongs to the authors.

Acknowledgements or Notes

This article was presented as an oral presentation at the International Conference on Research in Engineering, Technology and Science (www.icrets.net) conference held in Baku/Azerbaijan on July 01-04, 2022.

References

- Altintig, E., Onaran, M., Sari, A., Altundag, H., & Tuzen, M. (2018). Preparation, characterization and evaluation of bio-based magnetic activated carbon for effective adsorption of malachite green from aqueous solution. *Materials Chemistry and Physics*, 220(January), 313–321.

- <https://doi.org/10.1016/j.matchemphys.2018.05.077>
- Dargahi, A., Samarghandi, M. R., Shabanloo, A., Mahmoudi, M. M., & Nasab, H. Z. (2021). Statistical modeling of phenolic compounds adsorption onto low-cost adsorbent prepared from aloe vera leaves wastes using CCD-RSM optimization: effect of parameters, isotherm, and kinetic studies. *Biomass Conversion and Biorefinery*. <https://doi.org/10.1007/s13399-021-01601-y>
- Dastkhon, M., Ghaedi, M., Asfaram, A., Goudarzi, A., Langroodi, S. M., Tyagi, I., ... Gupta, V. K. (2015). Ultrasound assisted adsorption of malachite green dye onto ZnS:Cu-NP-AC: Equilibrium isotherms and kinetic studies - Response surface optimization. *Separation and Purification Technology*, 156, 780–788. <https://doi.org/10.1016/j.seppur.2015.11.001>
- Deb, A., Debnath, A., & Saha, B. (2021). Sono-assisted enhanced adsorption of eriochrome Black-T dye onto a novel polymeric nanocomposite: kinetic, isotherm, and response surface methodology optimization. *Journal of Dispersion Science and Technology*, 42(11), 1579–1592. <https://doi.org/10.1080/01932691.2020.1775093>
- Eltaweil, A. S., Ali Mohamed, H., Abd El-Monaem, E. M., & El-Subruiti, G. M. (2020). Mesoporous magnetic biochar composite for enhanced adsorption of malachite green dye: Characterization, adsorption kinetics, thermodynamics and isotherms. *Advanced Powder Technology*, 31(3), 1253–1263. <https://doi.org/10.1016/j.apt.2020.01.005>
- Gadekar, M. R., & Ahammed, M. M. (2019). Modelling dye removal by adsorption onto water treatment residuals using combined response surface methodology-artificial neural network approach. *Journal of Environmental Management*, 231(October 2018), 241–248. <https://doi.org/10.1016/j.jenvman.2018.10.017>
- Gandha, K., Mohapatra, J., Hossain, M. K., Elkins, K., Poudyal, N., Rajeshwar, K., & Liu, J. P. (2016). Mesoporous iron oxide nanowires: Synthesis, magnetic and photocatalytic properties. *RSC Advances*, 6(93), 90537–90546. <https://doi.org/10.1039/c6ra18530d>
- Gautam, R. K., Rawat, V., Banerjee, S., Sanroman, M. A., Soni, S., Singh, S. K., & Chattopadhyaya, M. C. (2015). Synthesis of bimetallic Fe-Zn nanoparticles and its application towards adsorptive removal of carcinogenic dye malachite green and Congo red in water. *Journal of Molecular Liquids*, 212, 227–236. <https://doi.org/10.1016/j.molliq.2015.09.006>
- Giri, S. K., Das, N. N., & Pradhan, G. C. (2011). Magnetite powder and kaolinite derived from waste iron ore tailings for environmental applications. *Powder Technology*, 214(3), 513–518. <https://doi.org/10.1016/j.powtec.2011.09.017>
- Gunduz, F., & Bayrak, B. (2018). Synthesis and performance of pomegranate peel-supported zero-valent iron nanoparticles for adsorption of malachite green. *Desalination and Water Treatment*, 110, 180–192. <https://doi.org/10.5004/dwt.2018.22185>
- Harja, M., Buema, G., & Bucur, D. (2022). Recent advances in removal of Congo Red dye by adsorption using an industrial waste. *Scientific Reports*, Vol. 12. <https://doi.org/10.1038/s41598-022-10093-3>
- Irfan, H., Mohamed Racik, K., & Anand, S. (2018). Microstructural evaluation of CoAl₂O₄ nanoparticles by Williamson–Hall and size–strain plot methods. *Journal of Asian Ceramic Societies*, 6(1), 54–62. <https://doi.org/10.1080/21870764.2018.1439606>
- Kahouli, M., Barhoumi, A., Bouzid, A., Al-Hajry, A., & Guermazi, S. (2015). Structural and optical properties of ZnO nanoparticles prepared by direct precipitation method. *Superlattices and Microstructures*, 85, 7–23. <https://doi.org/10.1016/j.spmi.2015.05.007>
- Karacabey, P., Döven, S., Uzunoglu, D., & Özer, A. (2019). Synthesis of 3D Hierarchical Flower-like MgO Microstructure: Investigation of its Adsorption and Antibacterial Properties. *Arabian Journal for Science and Engineering*, 44(12). <https://doi.org/10.1007/s13369-019-03959-8>
- Kargin, J., Valladares, L. D. L. S., Borja-Castro, L. E., Xize, J., Mukhambetov, D. G., Konyukhov, Y. V., ... Barnes, C. H. W. (2022). Characterization of iron oxide waste scales obtained by rolling mill steel industry. *Hyperfine Interactions*, 243(1), 1–11. <https://doi.org/10.1007/s10751-022-01800-7>
- Khuyen, H. T., Huong, N. T., Huong, T. T., Lien, P. T., Chi, T. K., Thi, V., Tung, D. K. (2018). Luminescent – Magnetic Nanoparticle and Their Properties. *IEEE Transactions on Magnetics*, 54(6), 4–7.
- Kiani, G., Dostali, M., Rostami, A., & Khataee, A. R. (2011). Adsorption studies on the removal of Malachite Green from aqueous solutions onto halloysite nanotubes. *Applied Clay Science*, 54(1), 34–39. <https://doi.org/10.1016/j.clay.2011.07.008>
- Liang, W., Li, D., Ma, X., Dong, W., Li, J., Wu, R., ... Dong, Q. (2018). Surface β -cyclodextrin polymer coated Fe₃O₄ magnetic nanoparticles: Synthesis, characterization and application on efficient adsorption of malachite green. *Journal of Nano Research*, 54, 54–65. <https://doi.org/10.4028/www.scientific.net/JNanoR.54.54>
- Nguyen, V. T., Vo, T. D. H., Nguyen, T. B., Dat, N. D., Huu, B. T., Nguyen, X. C., ... Bui, X. T. (2022). Adsorption of norfloxacin from aqueous solution on biochar derived from spent coffee ground: Master variables and response surface method optimized adsorption process. *Chemosphere*, 288(P2), 132577.

<https://doi.org/10.1016/j.chemosphere.2021.132577>

- Patra, J. K., & Baek, K. H. (2014). Green Nanobiotechnology: Factors Affecting Synthesis and Characterization Techniques. *Journal of Nanomaterials*, 2014. <https://doi.org/10.1155/2014/417305>
- Roosta, M., Ghaedi, M., Shokri, N., Daneshfar, A., Sahraei, R., & Asghari, A. (2014). Optimization of the combined ultrasonic assisted/adsorption method for the removal of malachite green by gold nanoparticles loaded on activated carbon: Experimental design. *Spectrochimica Acta - Part A: Molecular and Biomolecular Spectroscopy*, 118, 55–65. <https://doi.org/10.1016/j.saa.2013.08.082>
- Schoeman, Y., Oberholster, P., & Somerset, V. (2021). A zero-waste multi-criteria decision-support model for the iron and steel industry in developing countries: A case study. *Sustainability (Switzerland)*, Vol. 13, pp. 1–23. <https://doi.org/10.3390/su13052832>
- Shalaby, S. M., Madkour, F. F., El-Kassas, H. Y., Mohamed, A. A., & Elgarahy, A. M. (2021). Green synthesis of recyclable iron oxide nanoparticles using *Spirulina platensis* microalgae for adsorptive removal of cationic and anionic dyes. *Environmental Science and Pollution Research*, 28(46), 65549–65572. <https://doi.org/10.1007/s11356-021-15544-4>

Author Information

Deniz Uzunoglu

Department of Chemical Engineering, Faculty of Engineering, Mersin University, Mersin, 33343, Turkey
Contact e-mail: denizuzunoglu4@gmail.com

Ayla Ozer

Department of Chemical Engineering, Faculty of Engineering, Mersin University, Mersin, 33343, Turkey

To cite this article:

Uzunoglu, D. & Ozer, A. (2022). Synthesis of iron-containing nanoparticles from iron-steel industrial waste for adsorption of malachite green. *The Eurasia Proceedings of Science, Technology, Engineering & Mathematics (EPSTEM)*, 17, 6-18.